URSI GASS 2021,Rome, Italy,28 August- 4September 2021

Cosmic Noise Absorption Characteristics during the Impulse-Induced Supersubstorm of 21st January 2005

Shipra Sinha*[1], Geeta Vichare[1], Sneha Gokani[2], A. K. Sinha[1], Harald U. Frey [3], Rahul Rawat[1] , Gopi Seemala[1] and Antti Kero[4]

[1]Indian Institute of Geomagnetism, New Panvel (W), Navi Mumbai, India.
[2]State Key Laboratory of Marine Geology, Tongji University, Shanghai, China
[3]Space Sciences Laboratory, University of California, Berkeley, CA 94720, USA
[4]Sodankylä Geophysical Observatory, Tähteläntie 62, Sodankylä, Finland

Abstract

The impulse-induced super substorm of 21st January 2005 has been reported by Hajra and Tsurutani (2018) and they have discussed the abnormal morphology of the auroral dynamics mainly examining the auroral images and currents. This event is revisited here with additional datasets of global Cosmic Noise Absorption (CNA) by Riometers, auroral images by a space-based Imager, plasma flux data from geostationary satellites and magnetic field measurements of ground stations covering almost all latitudinal and local time sectors. We have observed some peculiar characteristics of this event: (1) No southward component of IMF Bz prior to the substorm onset. (2) Westward electrojet current peaks in the dawn sector, and not in the midnight sector, during the substorm interval. (3) Presence of dayside shock-auroras: The electron & proton auroras are stronger in the pre and post-midnight sectors and strongest on the dayside. (4) The time of CNA onset and substorm onset coincide in the narrow belt of magnetic latitude near 65°. The time delay between these two increases away from this belt on both-poleward and equatorward latitudes. The delay is small (~ 2 minutes) on the dayside and significant (~ 11 minutes) on the night side. (5) The percentage of CNA is found to vary with MLT as well as with latitudes. CNA absorption is lowest on the dayside (~ 20%) whereas near dawn and dusk the percentage of CNA is nearly equal (~40-50%). (6) Considering the model proposed by Sorathia et al. (2019) we can say that the dawn-dusk symmetry observed in the CNA indicates the entry of particles from the flanks facilitated by Kelvin-Helmholtz instability.

1 Introduction

Polar magnetic substorms are observed as large-scale geomagnetic perturbations generally being accompanied by an enhancement in particle precipitation, ionospheric absorption and disruption of the auroral arc structure (Rostoker, 1968). The behavior of auroral evolution, auroral electrojet current and substorm associated cosmic noise absorption are expected to be concomitant, all being dominant in the midnight sector during substorms. The reconnection in the magnetotail results into the release of this stored magnetotail energy into the auroral zones. It is shown that in general for a substorm to occur; precursor southward interplanetary magnetic fields are necessary ~1.5 hr prior to shock impingement (Zhou & Tsurutani, 2001). However, Rostoker (1968) concluded that a southward-directed interplanetary magnetic field is necessary or favorable but not the sufficient condition for the generation of magnetospheric substorm. In fact, there are evidences which show that substorms can occur even without southward turning of IMF. Kawasaki et al. (1971) showed that a sudden compression of the magnetosphere alone, if intense enough, can sometimes trigger substorms.

Supersubstorms (SSS) are extremely intense substorms with SuperMAG AL (SML) peak intensity ≤ -2500 nT and can last for several hours (Tsurutani et al., 2015). Hajra and Tsurutani (2018) reported the impulse induced supersubstorms of 21st January 2005 arguing that the magnetospheric energy input through magnetic reconnection either prior to the shock arrival or during the event was insufficient to power this event. In this paper, this event is revisited with additional database of global cosmic noise absorption (CNA) data, electron and proton auroral images, plasma flux data from geostationary satellites and magnetic field measurements covering almost all the available latitudinal and local time sectors. Unlike Hajra and Tsurutani (2018), we are concentrating only near the substorm onset, where the IMF Bz is northward and there is no possibility of magnetic reconnection at the subsolar dayside magnetopause.

2 Observation

2.1 Event description

Figure 1 shows the interplanetary and geomagnetic condition on 21st January 2005. The onset of SSS was at 17:11 UT with a sharp decrease in AL index indicated by the black solid vertical arrow. The second panel (b) shows that the IMF was almost 0 for several hours prior to the substorm onset. This shows that the IMF had no

southward component before the substorm onset, suggesting this supersubstorm not to be associated with magnetic reconnection. Panel (a), (c) and (d) shows a sudden increase in the solar wind ram pressure, velocity, and proton density; indicating shock arrival at the time of onset. Hence, this SSS was considered to be impulse induced (Hajra et al., 2018).

2.2 Cosmic Noise Absorption (CNA)

In Figure 2 the CNA curve of all the Riometer stations under study are divided into two panels. The left panel includes plots of the stations which lie in the dayside at the time of substorm onset and the right panel includes plots of the stations lying in the night-side at that time. All the stations are arranged according to their latitudes, starting from sub-auroral and moving towards polar. Black vertical arrow shows the time of substorm onset. Before the onset we do not see much variation in the absorption curves. After the substorm onset we observed absorption onset in these locations which is marked with sudden increase in each curve. The substorm and the CNA onsets coincide in the auroral region of day-side as well as night-side. Whereas, the absorption onset shows a delay from the substorm onset as we move away either towards the pole or towards the equator. Green curves show CNAs of stations with immediate absorption onset and pink curve shows CNAs of stations having delay in absorption from the substorm onset. The figure indicates that the enhancement in the ionization of the D-region took place simultaneously with the substorm onset in the auroral region only, and this happened at all longitudes.

To check how the intensity of the CNAs varies, we calculated the percentage absorption at different MLT using the formula:

$$\text{Percentage Absorption} = (\text{CNA}/\text{QDC}) * 100\ \% \quad (1)$$

Where,

CNA is the absorption magnitude (in dB) of a disturbed day of a month, and QDC is the quiet day value (in dB) at the same magnetic local time but on quiet days of the same month. Equation 1 gives an idea of how much absorption has taken place compared to a quiet day. This parameter helps in comparing the absorption strength of two or more stations which we cannot do using simple CNA values due to the fact that the quiet day values are different for different locations. Figure 3 shows variation in CNA percent at different local time in the latitudinal belt of 64°-69°. In order to check how the instantaneous particle precipitation was distributed in the local time sectors, stations showing no delay are taken into account in this plot. The percentage absorption is almost the same in the dawn and dusk sector having values around 40-50%, whereas in the dayside it is around 20%. Solar wind particles entering the magnetosphere during northward IMF are dawn-dusk symmetric when they enter from the flanks and are facilitated mainly by Kelvin-Helmholtz instability (Sorathia et al., 2019). The present substorm appears to be one such case where the particles have entered from the flanks. Generally, in an Akasofu-type substorm where particles enter from the midnight sector following the field lines, maximum and instantaneous absorption is observed in the midnight sector unlike the present case.

2.3 Auroral and Satellite Observation

We also checked the auroral images to see whether the signature matches with CNA and electrojet current behavior. Figure 4 shows global view of aurora in three wavelength range, viz., 121.8 nm, 135.6 nm and 140-180 nm. These auroral images were taken by NASA's Imager for Magnetopause-to-Aurora Global Exploration (IMAGE; Mende et al., 2000) satellite. The first panel of this figure shows auroras of 135.6 nm wavelength (oxygen OI emission), which is generated mostly by electrons with a little contribution of energetic protons (Frey et al., 2003). The second panel shows 121.8 nm aurora generated by protons only. The third panel shows wideband auroral images of 140-180 nm wavelength which is due to molecular nitrogen excitation. The images are at ~17:11, ~17:13 and ~17:15 UT marking the onset and emergence of aurora predominantly in the day time sector. The most intense aurora is in the dayside covering a wider latitude range as compared to other time sectors which also explains why we see more cosmic noise absorption in the dayside with higher latitudinal coverage area.

We observe form Figure 5 that LANL-94 which was in the dawn sector shows sudden enhancement in the electron flux of energy range 315-1500 keV. GOES-10 which is slightly ahead of LANL-94 towards the morning sector shows a sudden drop in the electron flux of energy range >0.6 MeV. LANL-90 which is in the post-noon sector also shows instantaneous decrement in electron flux of energy range 315-1500 keV. Whereas, LANL-97 which is in the post-midnight shows no change at 17:11 UT. The enhancement evident at 17:23 UT in LANL-97 could be due to the second impulse which occurred at that time. The sudden enhancement in the dawn sector may be due to the injection of particles. The decrement in the relativistic electron flux on the dayside magnetosphere i.e. morning and post noon sector may indicate dropout events. The dropout events could be due to loss of electrons from the outermost radiation belt into space during sudden compression of the magnetosphere known as magnetopause shadowing, or the electrons can be knocked down into the atmosphere due to wave-particle interaction. The precipitation of the plasmaspheric particles along the field lines into the atmosphere can be the source of sudden increase in the CNA.

3 Discussion

There have been number of modeling efforts to study the solar wind plasma transport via KHI. Using a combination of global magnetohydrodynamic and test particle simulations, Sorathia et al., (2019) compared the solar wind ion entry into the magnetosphere during northward

IMF via KHI and through cusp reconnection mechanisms. They found that both entry mechanisms provide comparable mass but affect entering plasma differently. The flank-entering plasma is dawn-dusk symmetric, whereas the cusp-entering plasma is accelerated and preferentially deflected toward dawn, producing dawn-dusk asymmetry. Our results indicate that the percentage of CNA absorption is lowest on the dayside, and the percentage is almost equal on dawn and dusk regions. This dawn-dusk symmetric CNA absorption intensity may be indicative of the role of KHI mechanism in the studied impulse-induced SSS event on 21st January 2005 in the auroral belt of 64°-69°. Further, Sorathia et al., (2019) reported that ~1/3 and ~2/3 of the entering mass takes place via flank-entering and cusp-entering mechanisms respectively. The flank-entering particles enter the magnetosphere in a near-equatorial region downtail from the subsolar point. They found that both these entry mechanisms exhibit quasi-periodic variability of 2–3 min for flank entry and ~8 min for cusp entry. Our results of high latitude time delay could be due to the time scales of cusp entry.

Thus, this paper reports observations which contradict the existing theory of substorms. The present work reveals a number of important observations related to the impulse-induced substorm, particularly near the substorm onset when the IMF was not southward. It also provides the observational evidence of the KH instability mechanism for the entry of particles during northward IMF. The SSS of 21st January 2005 do not only have a unique evolution process, but also has its prominent signatures in the dawn sector which otherwise are expected to be observed in the midnight sector. In order to understand more about such events, similar detailed multi instrument analysis, both ground based and satellite based, of impulse induced substorms are required in future.

4 Figures

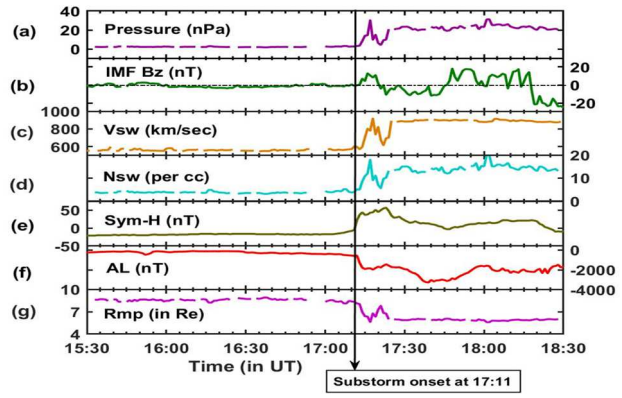

Figure 1. Interplanetary condition and geomagnetic parameters during SSS event of 21 January 2005. From top to bottom, the panels show (a) solar wind ram pressure (in nPa), (b) interplanetary magnetic field Z component (IMF Bz in nT) in GSM coordinates, (c) solar wind speed (Vsw in km/s), (d) solar wind proton density (Nsw in cm^{-3}), (e) SYM-H (nT), (f) AL (nT), (g) Magnetopause standoff distance (Rmp in terms of Re). Onset of the SSS event at 17:11 UT is indicated by the vertical solid black arrow.

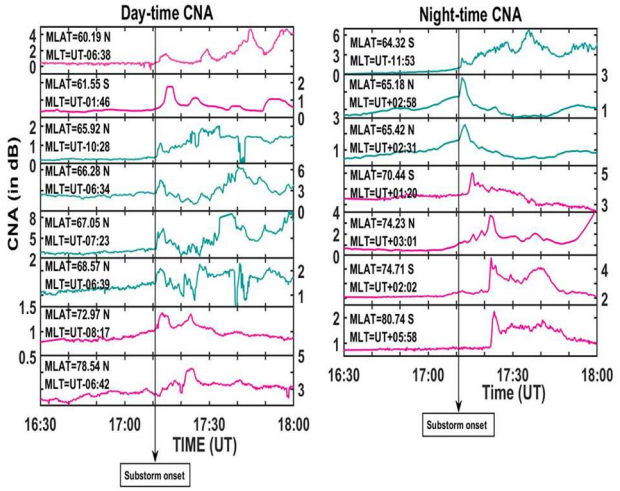

Figure 2: The right column of the figure has CNA observations of stations lying in the nightside during the time of substorm onset, and the left column has stations that lie in the dayside. In each column the stations are arranged in ascending order of their magnetic latitude, starting from sub-auroral to polar latitude from top to bottom. The X-axis shows time in UT and the Y-axis of each panel shows absorption in dB. The vertical arrow indicates the time of substorm onset.

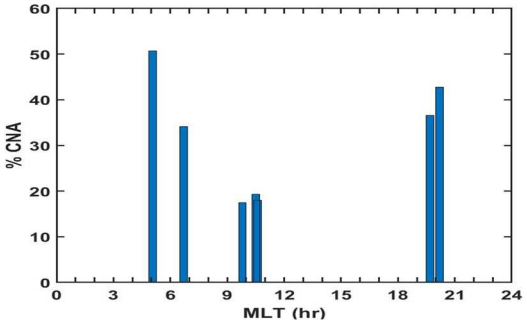

Figure 3: Local time variation of % CNA absorption in a latitudinal belt of 64-69 deg.

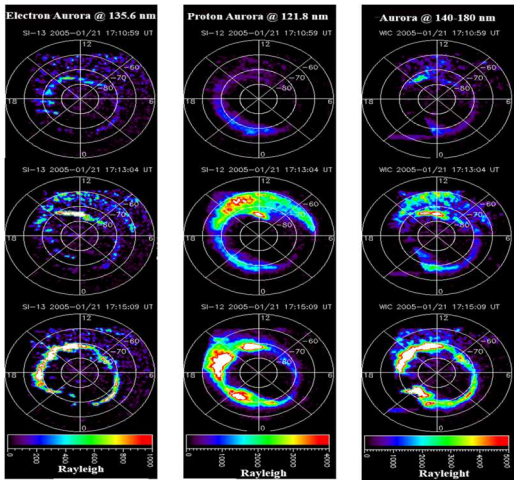

Figure 4: Global view of aurora by IMAGE satellite on 21st January 2005. First panel shows Electron Auroral Images in Far Ultraviolet (FUV) range (135.6 nm) taken by Spectrographic Imaging Camera. Second panel shows Proton Auroral Images in FUV range (121.8 nm) taken by Spectrographic Imaging Camera. Third panel shows Auroral Images in FUV range (140-180 nm) taken by Wideband Imaging Camera (WIC). Images are shown from ~17:11 UT to ~17:15 UT at an interval of two minutes.

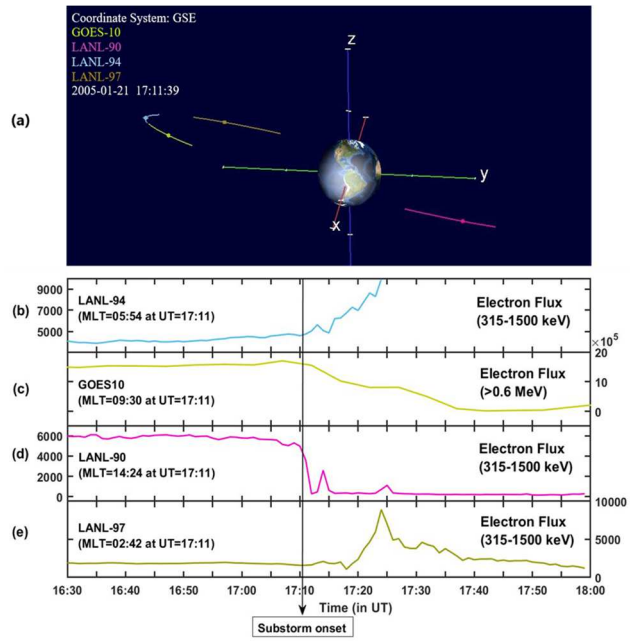

Figure 5. (a) The orbital view of GOES10, LANL-90, LANL-94 and LANL-97 obtained from NASA's 4-D orbit viewer software (https://spdf.gsfc.nasa.gov/data_orbits.html). The sun is in the positive x-direction. The duration of the plot is from 16:30 UT to 18:00 UT and the dots indicate satellite position at 17:11 UT. **(b)** Electron flux of LANL-94 of energy range 315-1500 keV (in e/(keV*cm^2*Sr*sec)), **(c)** Electron flux of GOES10 in the energy range >0.6 MeV (in e/($cm^2 * s * Sr$)), **(d)** Electron flux of LANL-90 of energy range 315-1500 keV (in e/(keV*cm^2*ster*sec)) and **(e)** Electron flux of LANL-97 of energy range 315-1500 KeV (in e/(keV* cm^2 *ster*sec)). Black vertical arrow indicates the time of substorm onset.

5 Acknowledgements

This work is carried out at Indian Institute of Geomagnetism, and supported by the Department of Science and Technology, Government of India. Authors would like to thank all of their data providers. Authors acknowledge Space Physics Data Facility (http://spdf.gsfc.nasa.gov/) for IMAGE auroral data and (https://spdf.gsfc.nasa.gov/data_orbits.html) for 4D orbit viewer software, CDAweb (cdaweb.gsfc.nasa.gov/) for providing interplanetary observations and satellite datasets; and SuperMAG (http://supermag.jhuapl.edu/) for providing magnetic data. Authors also deeply acknowledge NORSTAR (http://aurora.phys.ucalgary.ca/norstar/rio/index.html), Sodankylä Geophysical Observatory (https://www.sgo.fi/Data/Riometer/rioStation.php) and Australian World Data Centre (https://www.sws.bom.gov.au/World_Data_Centre/2/4) for high latitude Riometer datasets.

6 References

1. Frey, H.U., S.B. Mende, T.J. Immel, J.-C. Gerard, B. Hubert, S. Habraken, J. Spann, G.R. Gladstone, D.V. Bisikalo, V.I. Shematovich (2003). Summary of quantitative interpretation of IMAGE far ultraviolet auroral data, Space Science Reviews, 109, 255-283, 10.1023/B:SPAC.0000007521.39348.a5.

2. Hajra R., Tsurutani B. T. (2018). Interplanetary Shocks Inducing Magnetospheric Supersubstorms (SML<−2500nT): Unusual Auroral Morphologies and Energy Flow, *The Astrophysical Journal,* 858:123 (6pp), doi:10.3847/1538-4357.

3. Kawasaki, K., S.-I. Akasofu, F. Yasuhara, and C.-I. Meng (1971). Storm sudden commencements and polar magnetic substorms, *J. Geophys. Res.,* 76, 6781.

4. Mende, S.B., H. Heetderks, H.U. Frey, M. Lampton, S.P. Geller, S. Habraken, E. Renotte, C. Jamar, P. Rochus, J. Spann, S.A. Fuselier, J.-C. Gerard, R. Gladstone, S. Murphree, L. Cogger (2000). Far ultraviolet imaging from the IMAGE spacecraft: 1. System design, Space Science Reviews, 91, 243-270, 10.1023/A:1005271728567, 2000

5. Rostoker, G. (1968). Relationship between the Onset of a Geomagnetic Bay and the Configuration of the Interplanetary Magnetic Field, *J. Geophys. Res.* vol 73, no. 13.

6. Sorathia, K., Merkin, V. G.,Ukhorskiy, A. Y., Allen, R. C.,Nykyri, K., & Wing, S. (2019). Solarwind ion entry into the magnetosphere during northward IMF. *Journal of Geophysical Research:Space Physics*, *124*, 5461–5481. https://doi.org/10.1029/2019JA026728

7. Tsurutani, B. T., R. Hajra, E. Echer, and J. W. Gjerloev (2015). Extremely intense (SML ≤ _2500 nT) substorms: Isolated events that are externally triggered, *Ann. Geophys. Commun.,* 33, 519–524, doi:10.5194/angeo-33-519-2015.

8. Zhou, X., Tsurutani B. T. (2001). Interplanetary shock triggering of nightside geomagnetic activity: Substorms, pseudobreakups, and quiescent events. *J. Geophys. Res.* Paper number2000JA003028, doi: 0148-0227/01/2000JA003028